

Multi-Wavelength Study of X-ray Pulsar 2S 1553-542 During Outburst in 2021

Manoj Mandal

Midnapore City College, Kuturia, Bhadutala, West Bengal, India 721129

and

Sabyasachi Pal

*Indian Centre for Space Physics, 43 Chalantika, Garia Station Road, Kolkata, India 700084
Midnapore City College, Kuturia, Bhadutala, West Bengal, India 721129*

ABSTRACT

We summarize the results of temporal and spectral analysis of the X-ray pulsar 2S 1553-542 using the Nuclear Spectroscopic Telescope Array (NuSTAR) and Swift during the outburst in January-February 2021. During the outburst, the spin period of the neutron star was $P = 9.2822 \pm 0.0001$ s based on NuSTAR data. The temporal evolution of the spin period, pulse profile, and pulse fraction is studied during the outburst. The spectra of the source are studied for different days of the outburst and can be well described by a model consisting of – a black body emission or a power law. We have investigated the inter-day evolution of different timing and spectral parameters during the outburst. The energy dependence of the pulse profile was studied to investigate the evolution of the individual peaks and emission geometry of the pulsar with a different energy. The pulse profile of the source shows strong single peak nature with a hump-like feature of relatively lower intensity and it evolves significantly with different energy ranges. The evolution of the pulse profile is studied during different phases of the outburst and the pulse fraction shows a positive correlation with energy.

Subject headings: accretion, accretion discs - stars: emission-line, pulsar: individual: 2S 1553-542.

1. Introduction

The X-ray transient 2S 1553-542 was discovered using Small Astronomy Satellite 3 (SAS-3) in 1975 (Apparao et al. 1978) during the Galactic plane survey. A strong pulsation

with the period of 9.3 was found (Kelley et al. 1983) with an orbital period P_{orb} of nearly 30 d (Pahari & Pal 2012).

During the outburst in 2007–2008, the spectral and timing properties of the X-ray pulsar were studied using RXTE. The RXTE allowed to improve the orbital parameters of the system and to trace the spectral evolution in the energy range 2.5–30 keV (Pahari & Pal 2012). During the outburst, the spin period P_{spin} was 9.2829 ± 0.0003 s with period derivative $\dot{P} \sim 10^{-9} \text{ s s}^{-1}$ and the pulsed fraction showed a negative correlation with the time of the outburst. The pulse profile was single-peaked, featureless and variability in pulse profile was observed during the outburst (Pahari & Pal 2012). Energy-dependent pulse profile was also studied but no significant variation of pulse profile with energy was found. Significant variability of pulse fraction was observed in RXTE/PCA observations and PF was decreased with the decay of the flaring activity. The power density spectrum showed an interesting feature, the fundamental line with its five harmonics was visible (Pahari & Pal 2012). The variation of different spectral parameters with different orbital phases was studied and it was shown that the source hard X-ray spectra in all available intensity states can be well explained with the combination of a broken power-law and blackbody component (with temperature varying between 2.5–4 keV) (Pahari & Pal 2012).

The X-ray pulsar 2S 1553-542 went through another outburst during 2015. During this outburst, the temporal and spectral properties of the source were studied using Chandra and NuSTAR data (Tsygankov et al. 2018). Based on the Fermi/GBM data, the orbital parameters of the system were substantially improved, which allowed determining the spin period of the neutron star $P = 9.27880(3)$ s and a local spin-up $\dot{P} = -7.5 \times 10^{-10} \text{ s s}^{-1}$ due to the mass accretion during the NuSTAR observations. Assuming accretion from the disc and using standard torque models, the distance to the system was estimated as $d = 20 \pm 4$ kpc. From the timing analysis, the single-peak shape pulse profile was found with a barely noticeable dependence on energy, which is quite similar to the previous results (Pahari & Pal 2012). The cyclotron absorption feature near 23.5 keV was found during the declining stage of the outburst with corresponding magnetic field strength $\sim 3 \times 10^{12}$ G (Tsygankov et al. 2018).

Recently the source went through an outburst after a quiescence of nearly six years as detected by Burst Alert Telescope (BAT) onboard Swift and Gas Slit Camera (GSC) onboard MAXI on January 2021 (Mandal & Pal et al. 2021). The X-ray flux started to increase from early January of 2021 and the duration of the outburst was nearly six weeks. We study the temporal and spectral properties of the X-ray pulsar in soft X-ray band using Swift/XRT and in hard X-ray band using NuSTAR. We study the evolution of the timing and spectral properties in 0.3–79 keV during the outburst in 2021 using Swift and NuSTAR

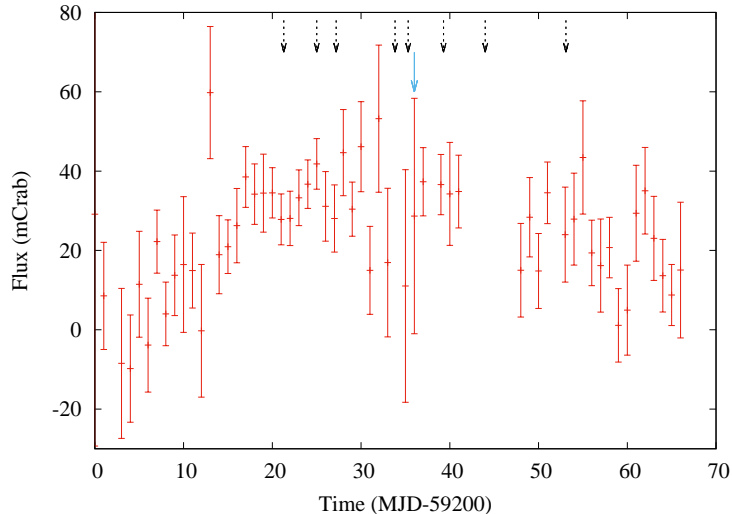


Fig. 1.— Outburst of 2S 1553-542 detected by Swift/BAT (15–50 keV) during January-February 2021. The blue solid arrow shows the time of NuSTAR observation and the black dotted-arrows show the time of Swift observations.

data. We study the variation of pulse period and pulse fraction over the outburst in the wide energy range (0.3–79 keV) and compare our results with the previous outbursts. We also look for the evolution of the pulse profile and dependence of the pulse profile on energy and luminosity. We have also studied the inter-day variation of different spectral parameters during the outburst.

We have discussed the data reduction and analysis method in Section 2. We have summarized the result of the current study in Section 3. The discussion and conclusion are summarized in the Section 4 and 5 respectively.

2. Observation and data analysis

We have detected an outburst from the X-ray pulsar and followed up using different. We use data from different all-sky X-ray monitors like Swift/BAT (15–50 keV), MAXI/GSC (2–20 keV), Fermi/GBM (12–25 keV) to study the evolution of the outburst. We analyzed the NuSTAR data close to the peak of the 2021 outburst and Swift/XRT data, which covers almost the whole outburst. We used the HEASOFT v6.27.2 for the data reduction and analysis.

2.1. Swift observations

Swift is primarily used for gamma-ray burst monitoring, and also useful in studying X-ray binaries in the energy range of 0.3–10 keV by using the X-ray telescope XRT (Gehrels et al. 2004). We used HEASOFT v6.27.2 for the reduction of Swift/XRT data. The summary of the Swift observations during the outburst is tabulated in Table 1. XRT data is processed and analyzed using the standard pipeline tool `xrtpipeline` v0.13.5 with the default screening criteria. From the clean event file, we have extracted the image using standard methods of `XSELECT` and the source and background were defined using `DS9`. The spectrum and light curve were extracted for the source and background using `XSELECT`. An ancillary response file (arf) was created for spectral analysis using `xrtmkarf` along with response matrix `swxpc0to12s6_20130101v014.rmf` for PC mode.

2.2. NuSTAR observations

The NuSTAR observatory comes with two co-aligned, identical X-ray telescope systems operating in a wide energy range of 3–79 keV. Separate solid-state CdZnTe pixel detector systems in each telescope usually referred to as focal plane modules A and B (FPMA and FPMB; Harrison et al. (2013)), have a spectral resolution of 400 eV at 10 keV and 900 eV at 68 keV (FWHM), respectively. NuSTAR performed an observation of 2S 1553-542 close to the peak of the outburst (MJD 59236.95) with a total exposure time of 28.35 ks (obs. id 90701302002). The observation log of NuSTAR is shown in the Table 1. The data is reduced using the NuSTARDAS pipeline version v0.4.7 (2019-11-14) provided under HEASOFT v6.27.2 with latest CALDB and we defined the source and background using `DS9` version 8.1. We extracted the light curve and spectra of the source and background from circular regions centering the source with radii of 50'' and 100'' using NUPRODUCTS scripts provided by the NuSTARDAS pipeline.

2.3. Fermi/GBM, Swift/BAT and MAXI/GSC observations

The Fermi Gamma-ray Space Telescope operates within a wide energy range between 8 keV–40 MeV. The Large Area Telescope (LAT) and Gamma-ray Burst Monitor (GBM) are two main instruments onboard the Fermi Gamma-ray Space Telescope (Meegan et al. 2009). The GBM is made up of 14 detectors: 12 detectors of Sodium Iodide (NaI) and 2 detectors of Bismuth Germanate (BGO). In the current study, we have used the spin frequency, frequency derivative, and 12–25 keV pulsed flux measurements with the Fermi/GBM

(Camero-Arranz et al. 2009; Finger et al. 2009). The outburst from 2S 1553-542 was also detected with Fermi/GBM from MJD 59200 and continued for nearly six weeks with a maximum pulsed flux of $\sim 0.21 \text{ keV cm}^{-2} \text{ s}^{-1}$ on MJD 59240.

BAT onboard the Swift observatory (Gehrels et al. 2004) is sensitive in hard X-ray (15-50 keV) (Krimm et al. 2013). We have used the results of the BAT transient monitor during the outburst, which is provided by the BAT team. BAT flux reached a maximum during the third week of January and continued for ~ 6 weeks.

We have made use of MAXI/GSC (2–20 keV) light curves data (Matsuoka et al. 2009) to follow up the outburst and to study the evolution of spectral states. MAXI in-orbit operation was started in 2009 and nearly 300 pre-registered sources have been monitored at a regular interval in different energy bands 2–4 keV, 4–10 keV, and 10–20 keV bands. The data provided by MAXI/GSC are averaged for every day. We have studied the evolution of hardness of the X-ray pulsar using data from different energy bands.

2.4. Timing analysis

The light curve has been extracted using the science event data in different energy ranges with bin sizes 0.1 s for both the modules (FPMA & FPMB) of NuSTAR. For Swift/XRT data, 2.5 s bin size was used. Basic filtering criteria and corrections were applied to get clean continuous science event data. We used the `efsearch` task in `FTOOLS` to check for the periodicity in the time series of the barycenter and background corrected data set. We used the folding method of the light curve over a trial period to get the best period by χ^2 maximizing process (Leahy 1987) over 32 phase bins in each period. After getting the best spin period, pulse profiles are obtained using `efold` task in `FTOOLS` by folding light curves with the best spin period. We also studied the power density spectrum of the source to detect the presence of Quasi-Periodic Oscillations (QPOs). Power density spectrum analysis was done using the `POWSPEC` routine of `FTOOLS` v6.27.2 which follows the FET algorithm. Power density spectra with bin time 0.1 s were created using event mode data in the energy range 3–79 keV. We also used the time-series data from the Fermi/GBM to study the evolution of the pulse period and pulsed flux during the outburst.

2.5. Spectral analysis

X-ray spectrum has been extracted using the Swift/XRT (1–10 keV) data with a bin time of 2.5 s. We excluded the spectrum above 10.0 keV and below 1.0 keV due to the poor source

count rate statistics in this range. The XRT spectra for different observations were fitted with the same model using XSPEC v12.11.0 and model parameters are varied independently. We have tried different simple single-component models like power-law, bbody, compTT as well as combinations of models like power-law+body, diskbb+bknpower, diskbb+compTT, compTT+bknpower, to fit the source spectrum perfectly. The spectrum can be well explained with a blackbody emission or power-law. To find the effect of absorption by hydrogen, all model components were multiplied by a photo-electric absorption model.

3. Results

The X-ray pulsar 2S 1553-542 went through an outburst during January-February 2021, detected by Fermi/GBM, Swift/BAT¹ and MAXI/GSC which reached a maximum flux during the last week of January 2021. Figure 1 shows the variation of flux during the outburst using Swift/BAT (15–50 keV). The total duration of the outburst was around 6 weeks which started in the first week of January 2021 and continued till the second week of February 2021. We have summarized the result of timing and spectral analysis of 2S 1553–542 during the recent outburst in 2021.

3.1. Evolution of pulse period and pulse profile during the outburst

We have investigated the evolution of the different timing parameters during the outburst using Swift and NuSTAR observations. The spin period of the pulsar during the outburst is $P = 9.2822 \pm 0.0001$ s using NuSTAR data, which is consistent with the pulse period evolution history as recorded with Fermi/GBM during the outburst² and the period is decreased slowly with the time of the outburst. Figure 2 shows the variation of normalized intensity over the phase during the outburst, which is single-peaked and nearly sinusoidal in the 3-79 keV energy range. An additional component of a hump-like feature with the strong single peak is detected during the NuSTAR observation for both the modules FPMA and FPMB.

We also looked for the energy dependence of pulse profiles as well as the temporal variation of pulse profile during the outburst. Figure 3 shows the energy-dependent pulse profiles for four different energy ranges. The variation of the pulse profile over four energy

¹<https://swift.gsfc.nasa.gov/results/transients/>

²<https://gammaray.nsstc.nasa.gov/gbm/science/pulsars>

Table 1: Log of NuSTAR and Swift observations

Instrument	Start time (MJD)	Date (yyyy-mm-dd)	Exposure (ks)	Observation id
NuSTAR	59236.95	2021-01-22	28.352	90701302002
Swift	59221.29	2021-01-07	1.353	00031096003 (Obs 1)
	59225.01	2021-01-11	1.250	00031096004 (Obs 2)
	59227.19	2021-01-13	1.293	00031096005 (Obs 3)
	59233.83	2021-01-19	1.311	00031096008 (Obs 4)
	59235.31	2021-01-21	1.435	00031096009 (Obs 5)
	59239.29	2021-01-25	1.595	00031096010 (Obs 6)
	59243.99	2021-01-29	1.296	00031096012 (Obs 7)
	59253.08	2021-02-08	0.849	00031096014 (Obs 8)

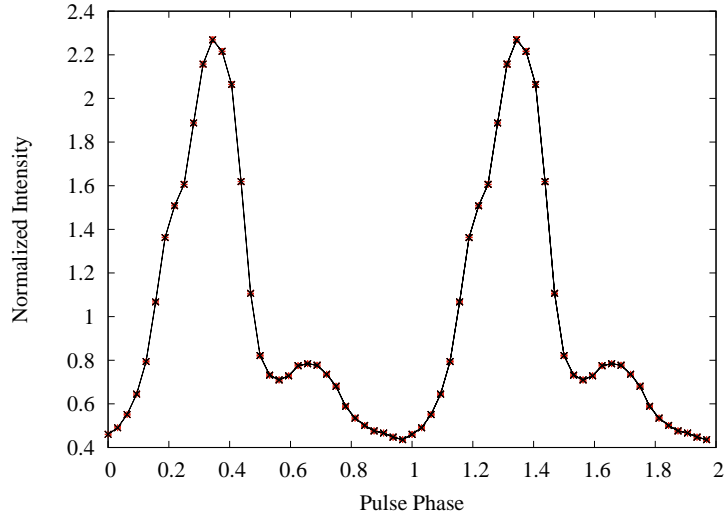


Fig. 2.— Variation of normalized intensity with the pulse phase using NuSTAR (3–79 keV). The pulse profile shows a prominent peak with a relatively weak hump.

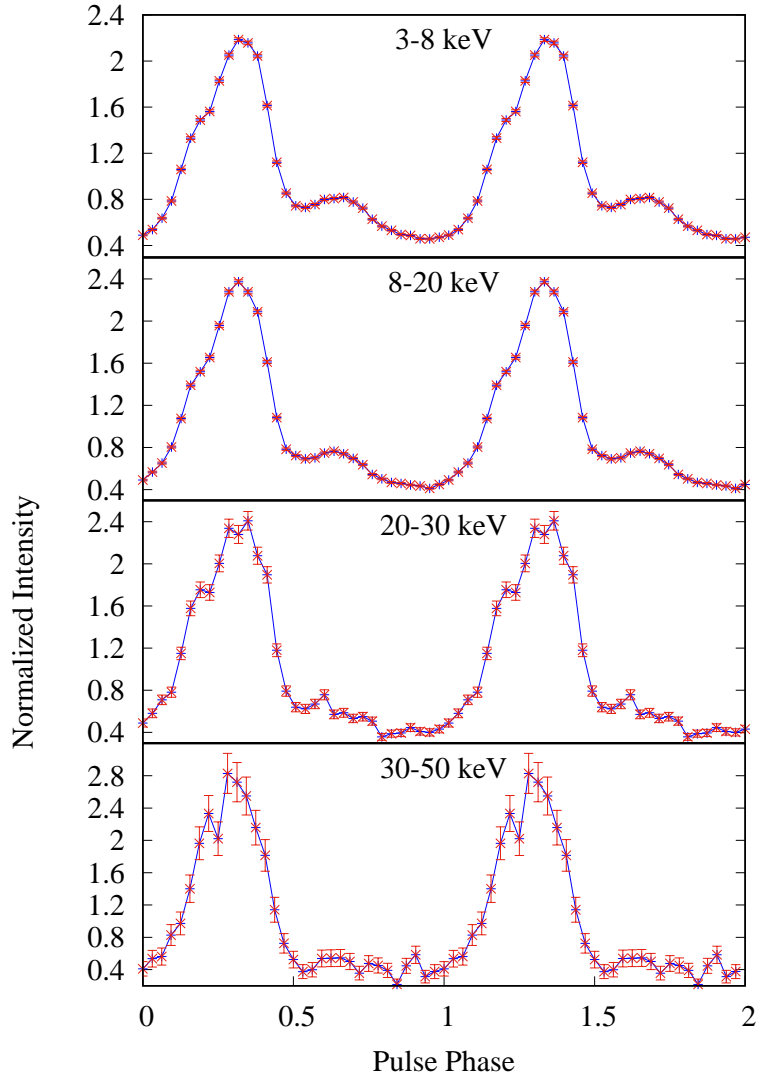


Fig. 3.— Energy dependent pulse profiles using data from NuSTAR observation.

Table 2: Power density spectrum fitting parameters with (constant + powerlaw + 6 Lorentzian components)

	Lorentzian centre (Hz)	Lorentzian width (mHz)
Fundamental	0.1076 ± 0.0001	1.13 ± 0.03
1st harmonic	0.2192 ± 0.0900	3.67 ± 0.17
2nd harmonic	0.3293 ± 0.0010	3.58 ± 0.72
3rd harmonic	0.4256 ± 0.0050	6.00 ± 1.91
4th harmonic	0.5320 ± 0.0040	11.00 ± 5.00
5th harmonic	0.6693 ± 0.0500	1.61 ± 0.80

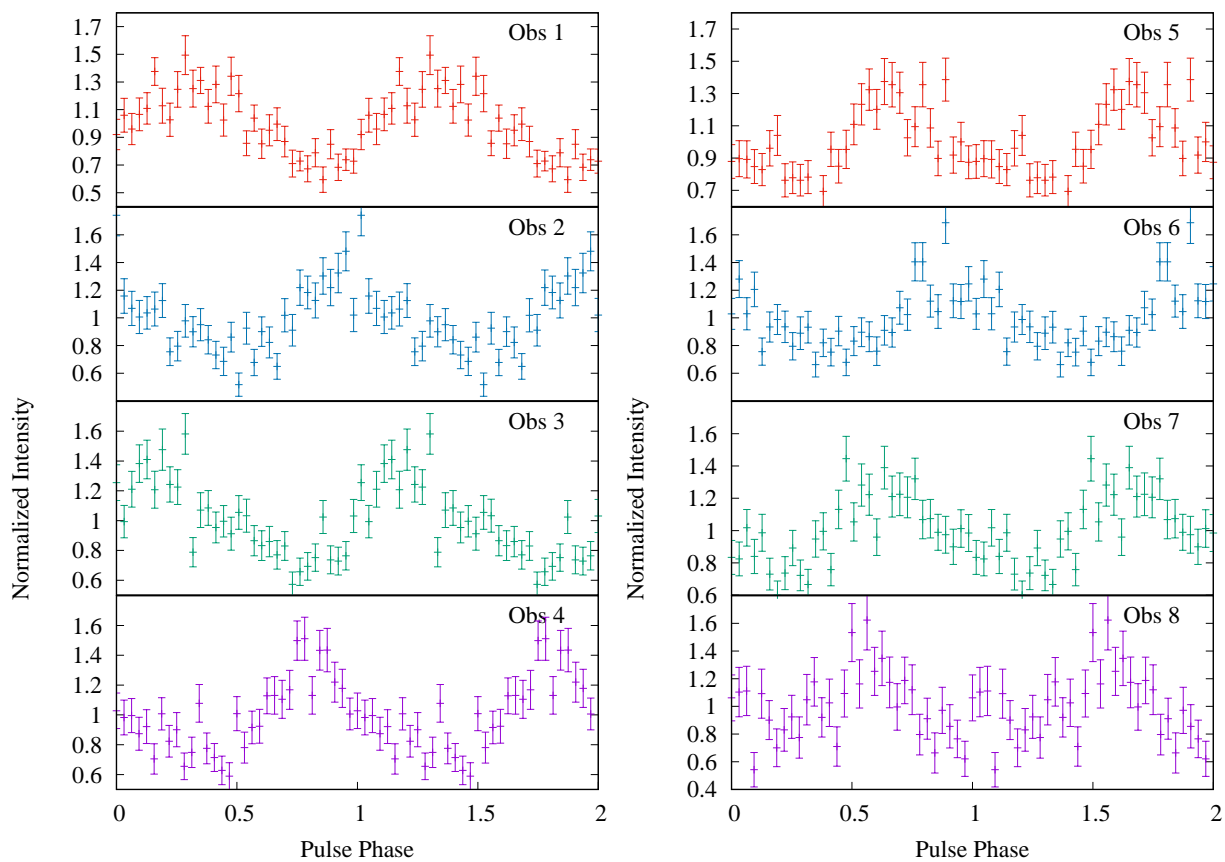


Fig. 4.— Temporal Variation of pulse profiles using Swift/XRT (0.3–10 keV): The variation of pulse profile in different days of outburst are shown in this figure.

bands: 3–8 keV, 8–20 keV, 20–30 keV and 30–50 keV is shown in Figure 3. The pulse profile shows a nearly sinusoidal nature, single-peaked, and an additional weak hump-like feature is observed. This feature changed significantly over different energy ranges. The shape of the pulse peak in the higher energy band (>20 keV) shows an additional component, which is more prominent in the 30–50 keV energy band.

The temporal evolution of pulse profile is also studied during the outburst using Swift/XRT. Figure 4 has shown the variation of pulse profiles during this outburst. The pulse profiles are more or less single-peaked and sinusoidal during the observations of the recent outburst.

The variation of Pulse Fraction (PF) with energy has also been studied during the NuSTAR observation. PF can be defined as the ratio between the difference of maximum intensity (I_{max}) and minimum intensity (I_{min}) to their sum: $[(I_{max} - I_{min}) / (I_{max} + I_{min})]$. Figure 5 shows the variation of PF for different energy ranges for which the energy-resolved pulse profile is studied and the horizontal bars represent the energy ranges for which the PF is calculated. The PF shows a positive correlation with energy. We have found that the pulse fraction increased from $\sim 66\%$ (3–8 keV) to $\sim 82\%$ (30–50 keV) during the outburst.

The right side panel of Figure 5 shows the variation of pulse fraction during the outburst using Swift/XRT data. The pulse fraction is varied between 40%–55% during the outburst and shows a trend to decrease its value during the declining phase of the outburst.

Figure 6 shows the evolution of the spin period and pulsed flux (12–25 keV) during the outburst using Fermi/GBM and the corresponding spin periods estimated from NuSTAR and Swift/XRT observations are shown in the upper panel of the figure. The figure implies that the pulse period of the X-ray pulsar has continuously decreased with time.

3.2. Power density spectrum

We have generated a Power Density Spectrum (PDS) with 0.1 s bin time light curves for both the module of NuSTAR – FPMA and FPMB independently in the energy range 3–79 keV. The power density spectrum is shown in Figure 7 along with the best-fitted model using NuSTAR data. Figure 7 shows the fundamental line at 0.1076 ± 0.0001 Hz with its five harmonics. The power density spectrum is well fitted with a model constant, power-law component (with a power-law index -0.35), and six Lorentzian components. The result of the best-fitted parameters of the power density spectrum with the model (constant + power-law + 6 Lorentzian components) is summarized in Table 2. This feature is more or less similar to the previous results during the 2007–2008 outburst as reported by Pahari & Pal (2012).

Table 3: Spectral fitting parameters for best fitted models for different Swift/XRT (1–10 keV) observations:

Model	Model Parameters	Obs 1	Obs 2	Obs 4	Obs 5	Obs 6	Obs 7
		59221.29	59225.01	59233.83	59235.31	59239.29	59243.99
Phabs*po	N_H , 10^{22} cm $^{-2}$	5.5 ± 0.6	4.6 ± 0.5	5.3 ± 0.6	5.8 ± 0.6	4.8 ± 0.5	5.1 ± 0.6
	Photon index (τ)	0.8 ± 0.1	0.6 ± 0.1	0.9 ± 0.1	0.9 ± 0.1	0.8 ± 0.1	0.7 ± 0.2
	χ^2 (d.o.f)	0.88 (896)	0.89 (896)	0.72 (896)	0.89 (896)	0.84 (896)	0.84 (896)
Phabs*bb	N_H , 10^{22} cm $^{-2}$	3.6 ± 0.4	2.8 ± 0.4	3.2 ± 0.4	$3.5 \pm 0.$	3.0 ± 0.3	3.2 ± 0.4
	kT_{bb} (keV)	2.3 ± 0.1	2.3 ± 0.1	2.0 ± 0.1	2.1 ± 0.1	2.1 ± 0.1	2.2 ± 0.2
	norm $_{bb}$, 10^{-3}	4.9 ± 0.4	4.8 ± 0.5	5.6 ± 0.4	3.8 ± 0.3	4.0 ± 0.3	4.4 ± 0.4
	χ^2 (d.o.f)	0.89 (896)	0.90 (896)	0.73 (896)	0.88 (896)	0.85 (896)	0.86 (896)
Flux (1–10 keV) 10^{-10} , ergs cm $^{-2}$ s $^{-1}$		2.4	2.3	3.0	1.9	2.1	2.2

N_H : Hydrogen column density, τ : power-law photon index, kT_{bb} : blackbody temperature

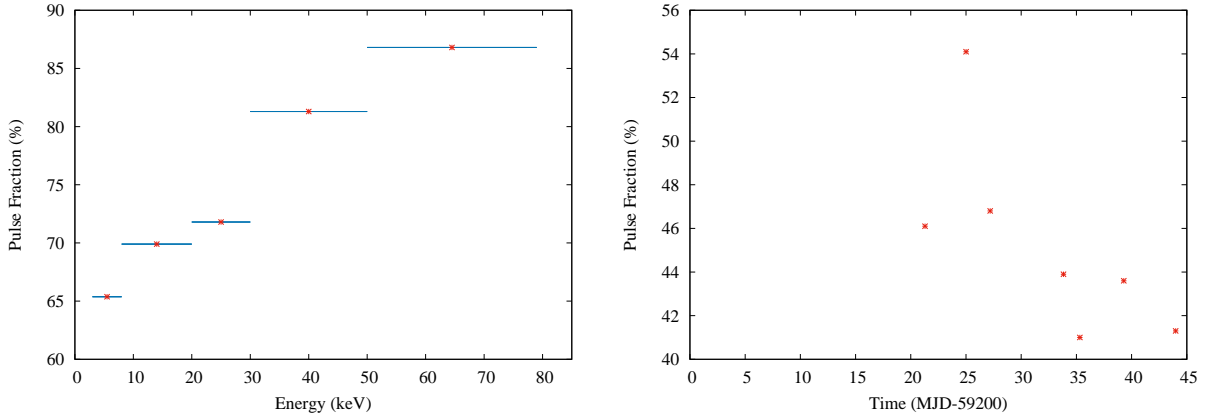


Fig. 5.— Left side shows the evolution of pulse fraction with energy using NuSTAR observation and the right side shows the evolution of pulse fraction during the outburst using Swift/XRT observations.

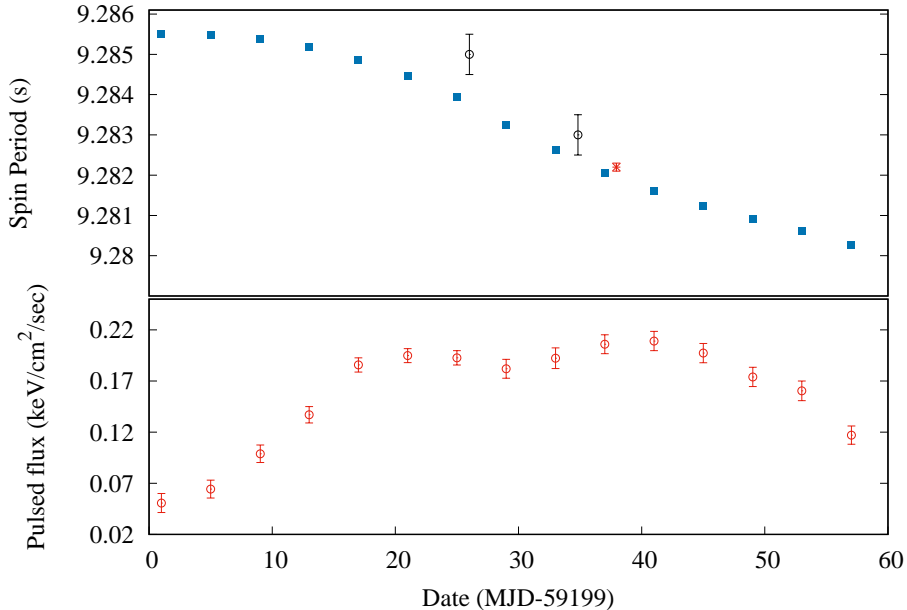


Fig. 6.— Variation of pulse period during the outburst. The blue rectangular symbols show the pulse period using Fermi/GBM and the red asterisk shows the pulse period calculated from NuSTAR observation and the black circles show the pulse periods estimated from Swift/XRT observations. The bottom panel shows the evolution of pulsed flux (12–25 keV) of Fermi/GBM. The vertical bars represent the error of corresponding measurements.

3.3. Energy spectrum

We have studied the energy spectrum for different days of the outburst using Swift/XRT observations and looked for the inter-day variation of different spectral parameters over the outburst. The energy spectrum with the best-fitted models is shown in Figure 8 where the bottom panels of the Figure 8 show the residuals. We extracted the energy spectrum for different observations from Swift/XRT and fitted them in XSPEC with varying the model parameters independently for different models. We have tried to fit the spectrum with simple models. The energy spectrum of the X-ray pulsar can be well fitted with a power-law (`powerlaw` in XSPEC) or blackbody emission component (`bbody` in XSPEC) along with a photoelectric absorption (`phabs` in XSPEC). The spectra in the energy range 1–10 keV are well described with blackbody emission with temperature ($kT_{bb} \sim 2.0$ keV) with Hydrogen column density $\sim 3.0 \times 10^{22} \text{ cm}^{-2}$. The spectra can also be well fitted with a power law with photon index ~ 0.6 and a neutral absorption of an equivalent hydrogen column density $\sim 5.0 \times 10^{22} \text{ cm}^{-2}$. The X-ray flux in the 1–10 keV energy range is $\sim 2.5 \times 10^{-10} \text{ ergs cm}^{-2} \text{ s}^{-1}$. Table 3 shows the evolution of different spectral parameters with the best-fitted values

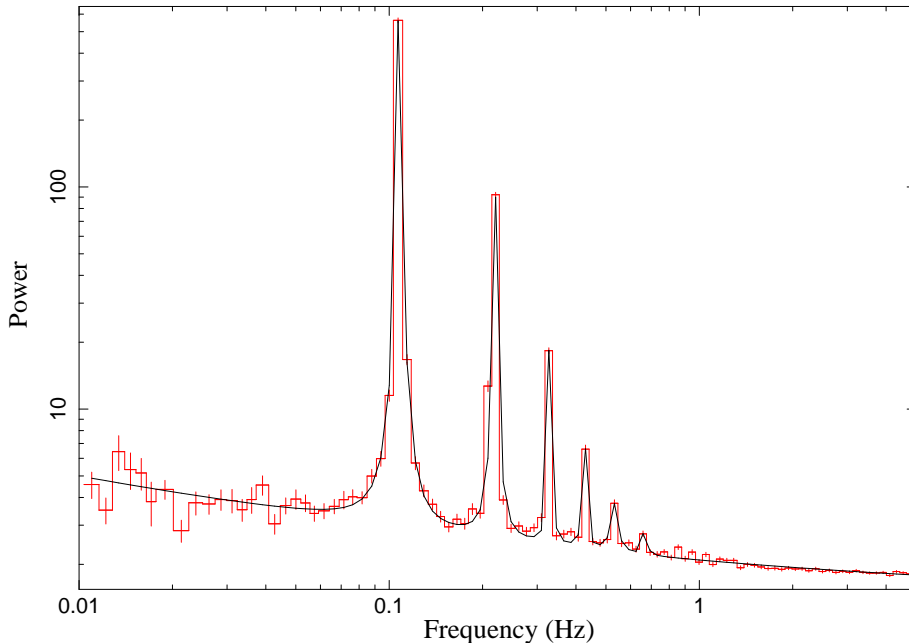


Fig. 7.— The power spectrum of 2S 1553-542 generated from the 0.1 s binned light curve over the energy band 3–79 keV using NuSTAR. The fundamental pulsation at 0.107 Hz with its five harmonics are clearly detected.

for different days of the outburst. The photon index is varied between ~ 0.6 – ~ 0.9 during different observations. The blackbody temperature (kT) is fluctuating between 2.0–2.3 keV during the different XRT observations.

4. Discussion

We have presented the result of timing and spectral analysis of 2S 1553-542 during the recent outburst in January-February 2021 using the NuSTAR and Swift data. The pulse profile is single-peaked and nearly sinusoidal, which is comparable to the previous outbursts in 2007–2008 (Pahari & Pal 2012) and 2015 (Tsygankov et al. 2018) and an additional hump-like feature along with the strong peak is prominent and shows an energy dependence. The energy dependence of the pulse profile was studied to investigate the evolution of the individual peaks and emission geometry of the pulsar with a different energy. The results showed an energy dependency of the additional hump-like feature which changes with energy from rela-

tively stronger in low energy to relatively weaker in higher energy. The pulse fraction shows a trend to increase with energy, which is typical for an X-ray pulsar (viz. Mandal & Pal (2020); Lutovinov & Tsygankov (2009)). We also study the temporal variability of pulse profile and pulse fraction during the outburst using Swift/XRT data from different observations. Previously the pulse fraction was varied with time during the outburst and decreased gradually with the outburst as observed by Pahari & Pal (2012). During the recent outburst, the PF is shown a negative correlation with time, which is similar to the result of the previous outburst in 2007–2008 Pahari & Pal (2012).

From the power density spectrum, we have detected the fundamental line along with five harmonics, which are fitted and explained with the same model as mentioned earlier. The fitting parameters of the harmonics closely match with the previous result during the 2007–2008 outburst (Pahari & Pal 2012).

We looked at the hardness ratio (HR) using the ratio of the count rates from Swift/BAT (15–50 keV) and MAXI/GSC (2–20 keV). The HR shows variability during the outburst and the HR is varied between ~ 0.5 –3 for the time MJD 59210–59265. The HR was also studied with MAXI/GSC (4–10 keV/2–4 keV) energy band, which also showed variability between ~ 0.7 –4.0 during the time MJD 59210–59265.

During the outburst, we also analyzed the ratio of the count rate from the Swift/BAT and the pulsed flux from the Fermi/GBM (12–25 keV) observations. During the time MJD 59212–59264, the ratio showed a significant variation, which suggests that during this period there was a significant change in the pulsed fraction.

The energy spectrum is studied using XRT in the 1–10 keV energy band and explained with simple model power-law or blackbody along with photoelectric absorption model. Earlier the X-ray spectrum of the source using XRT (0.5–10 keV) was modeled with simple model components like power-law and blackbody emission along with photoelectric absorption (Lutovinov et al. 2016). Previously, an iron emission line near 6.4 keV was reported from RXTE and NuSTAR observations (Pahari & Pal 2012; Tsygankov et al. 2018). We added a Gaussian component to the model to check the significance of the iron emission line and it did not improve the goodness of the fit of XRT observation. The evolution of different spectral parameters is studied during the several days of outburst, which suggest that the spectra from different XRT observations can be explained with a simple model like power-law along with photoelectric absorption or the black body emission along with photo absorption model which implies the emission mechanism may not vary significantly over the time during the outburst. Earlier, during 2007–2008 outburst the stability of spectral parameters in different orbital phase was observed by Pahari & Pal (2012) which is closely matched to our results during the recent outburst.

5. Conclusion

We have summarized the results of the timing and spectral analysis of the poorly studied X-ray pulsar during the outburst in 2021. The pulse profile shows single-peaked, sinusoidal nature, and a hump-like feature is observed which evolves significantly with energy. A positive correlation of PF with energy is observed and PF shows a trend to decrease with time during the outburst. The variation of the observed spin period is consistent with Fermi/GBM. The spectral model parameters were stable and do not show significant variation during the different phases of the outburst. The evolution of spectral parameters suggests that the emission mechanism is not varied over the time of the outburst.

Acknowledgements

This research has done using data collected by NuSTAR, a project led by Caltech, managed by NASA/JPL and funded by NASA, and has utilized the NUSTARDAS software package, jointly developed by the ASDC (Italy) and Caltech (USA). This research has made use of the MAXI data provided by the RIKEN, JAXA, and MAXI team.

Data availability

The data underlying this article are publicly available in the High Energy Astrophysics Science Archive Research Center (HEASARC) at

<https://heasarc.gsfc.nasa.gov/db-perl/W3Browse/w3browse.pl>.

REFERENCES

- Apparao K. M., Bradt H. V., Dower R. G., Doxsey R. E., Jernigan J. G., Li F., 1978, *Nat*, 271, 225
- Burrows D. N. et al., 2005, *Space Science Rev.*, 120, 165
- Camero-Arranz A., Finger M. H., Ikhsanov N. R., Wilson-Hodge C. A., Beklen E., 2009, *The Astrophysical Journal*, 708, 1500, 1506
- Finger M. H. et al., 2009, arXiv e-prints, p. arXiv:0912.3847
- Gehrels N. et al., 2004, *ApJ*, 611, 1005

- Harrison F. A. et al., 2013, *ApJ*, 770, 103
- Kelley R. L., Rappaport S., Ayasli S., 1983, *ApJ*, 274, 765
- Krimm H. A. et al., 2013, *ApJS*, 209, 114
- Leahy D. A., 1987, *A&A*, 180, 275
- Lutovinov A. A., Tsygankov S. S., 2009, *Astronomy Letters*, 35, 433
- Lutovinov A. A. et al., 2016, *MNRAS*, 462, 3823
- Mandal M., Pal S., 2020, arXiv e-prints, p. arXiv:2012.15839v 1 [astro-ph.HE]
- Mandal M., Pal S., Hazra M., 2021, *The Astronomer Telegram*, 14308,1
- Meegan C. et al., 2009, *ApJ*, 702, 791
- Matsuoka M. et al., 2009, *PASJ*, 61, 999
- Pahari M., Pal S., 2012, *MNRAS*, 423, 3352–3359
- Tsygankov S. S., Lutovinov A. A., Krivonos R. A., Molkov S. V., Jenke P. J., Finger M. H., Poutanenv J., 2016, *MNRAS*, 457, 258–266

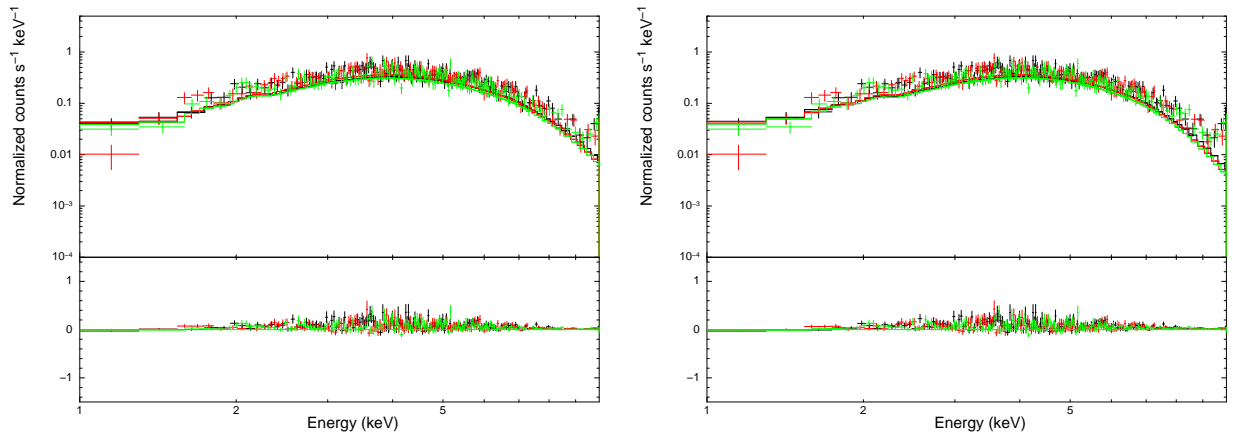


Fig. 8.— The left side figure shows the energy spectrum along with best-fitted model $\text{phabs} \times \text{power-law}$ for 3 different observations (obs 2, obs 4, obs 6) using Swift/XRT and the right side figure represents the energy spectrum with best-fitted model $\text{phabs} \times \text{blackbody}$. Residuals are shown in the bottom panel.